

# A functional relationship between capillary pressure, saturation, and interfacial area as revealed by a pore-scale network model

Paul C. Reeves and Michael A. Celia

Water Resources Program, Department of Civil Engineering and Operations Research, Princeton University  
Princeton, New Jersey

**Abstract.** The constitutive relationships required for the parameterization of multiphase flow and transport problems are of critical importance to hydrologic modeling. Recently, a hypothesis has been developed that predicts a functional relationship between capillary pressure, saturation, and interfacial area. A network model was developed to test this hypothesis. Microscale physical processes were simulated and volume averaging was used to derive the macroscopic measures of saturation and fluid-fluid interfacial area per volume of porous media. Results indicate that a smooth, though complex, functional relationship exists at the continuum scale. These results have direct relevance to constitutive theory and the modeling of nonaqueous phase liquid dissolution processes.

## Introduction

This paper presents results of a pore-scale network model simulator designed to explore the relationship between capillary pressure, saturation, and fluid-fluid interfacial area in a multifluid porous medium. Such a functional dependence has direct relevance to modeling interfacial mass transfer, including problems such as nonaqueous phase liquid (NAPL) dissolution. Experience has shown that fluid saturations alone are inadequate characterizations of the system state in attempts to model NAPL dissolution [e.g., Powers *et al.*, 1992; Miller *et al.*, 1990]; information regarding the distribution of the fluid phases is also required because it is the distribution of fluids at the pore scale that determines both the interfacial area between the fluid phases and the relative permeability of the medium to each fluid. These factors play an important role in regulating interfacial mass transfer and the transport of soluble species away from zones containing residual NAPL ganglia. Because of the difficulties inherent in measuring interfacial area, recent research has focused on the factors controlling ganglion size distributions and sought surrogate measures that can serve to characterize fluid distributions [e.g., Powers *et al.*, 1994a, b, 1992; Geller and Hunt, 1993; Parker *et al.*, 1991; Imhoff *et al.*, 1993; Mayer and Miller, 1992; Miller *et al.*, 1990]. In the present study, numerical results from a pore-scale network model are used to determine quantitatively a macroscopic relationship between capillary pressure, fluid saturations, and interfacial area between fluid phases.

This paper also provides an initial test of a hypothesis developed by Hassanizadeh and Gray [1990] that proposes a formal constitutive relationship between capillary pressure, saturation, and interfacial area. Such a functional dependence challenges the traditional constitutive relationship in which capillary pressure is a function of saturation alone, leading to the familiar hysteretic moisture retention function [e.g., Dullien, 1992]. (For the purposes of this paper, the “moisture retention function” refers to the relationship between capillary pressure and saturation, independent of the two fluids in-

involved.) Verification of the hypothesis of Hassanizadeh and Gray through physical experimentation will be an extremely difficult task because of the problems associated with measurements of the interfacial area between fluid phases in a three-dimensional, opaque, porous medium. Even if such an experiment can be designed and performed, it is possible that standard measurements on field cores may never be feasible. Computational multiphase network models offer an alternate, numerical means of performing such an “experiment” pending physical measurements or other computational approaches.

Network models were first developed by Fatt [1956] based on the idea that pore space may be represented as an interconnected network of capillary tubes whose radii represent the dimensions of the pores within a porous medium. Within the network of pores, proposed microscopic physical processes are simulated in order to model such behavior as the pore-by-pore displacement of immiscible fluids. The important benefit of such a modeling approach is that the geometry of all menisci in the system can be calculated. These fluid-fluid interfaces, along with the pore space geometry, completely determine the boundaries delineating the spatial distribution of fluids within the lattice. Given this information, macroscopic variables, such as fluid saturations and interfacial area per volume of porous medium, may be defined through geometric volume averaging. In this respect, network models can serve as a bridge between the microscopic and macroscopic scales.

Network models are now heavily used as investigative tools to study the nature of fluid flow from the perspective of the pore scale. They are used in petroleum engineering, chemical engineering, and physics and increasingly in hydrology. They have been used to study such topics as diffusion and dispersion [e.g., Hollewand and Gladden, 1992; Burganos and Payatakes, 1992; Sorbie and Clifford, 1991; Koplik *et al.*, 1988; de Arcangelis *et al.*, 1986], flow in fractures [e.g., Fourar *et al.*, 1993; Pyrak-Nolte *et al.*, 1992], pore-scale evaporation processes [Nowicki *et al.*, 1992], the formation and flow of foam [Laidlaw *et al.*, 1993], the interpretation of mercury porosimetry and associated characterization of pore size distributions [e.g., Ioannidis and Chatzis, 1993; Ioannidis *et al.*, 1993; Tsakiroglou and Payatakes, 1990; Chatzis and Dullien, 1985], and ganglion formation and mobilization [e.g., Dias and Payatakes, 1986; Li and Wardlaw, 1986a, b]. There have also been several network models de-

Copyright 1996 by the American Geophysical Union.

Paper number 96WR01105.  
0043-1397/96/96WR-01105\$09.00

veloped to study the constitutive relationships required to parameterize multiphase flow equations. The relative permeability-saturation function has been studied, primarily by petroleum engineers [e.g., *Bryant et al.*, 1993; *Blunt and King*, 1991; *Jerauld and Salter*, 1990; *Kantzas and Chatzis*, 1988]. The moisture retention function for both two- and three-phase systems has also received attention [e.g., *Soll and Celia*, 1993; *Zhou and Stenby*, 1993; *Maier and Laidlaw*, 1993, 1990; *Soll*, 1991; *Ferrand and Celia*, 1989, 1992a, b; *Li et al.*, 1986]. The network model algorithm used in this study borrows heavily on the algorithms and insights of these researchers and others. A review of the recent literature on network modeling is provided by *Celia et al.* [1995].

## Motivation

The constitutive relationships required for modeling flow and transport in multiphase systems are of critical importance to hydrologic modeling. It is through the incorporation of constitutive relationships into the flow equations that a simple mass balance statement is transformed into a system-specific formulation, i.e., specific to the particular porous medium and fluids present. Constitutive relationships also represent the point at which physical measurements are incorporated into mathematical and numerical models. In the case of two-phase flow, the required constitutive relationships in traditional models are the moisture retention function and the relative permeability-saturation function. Typically, the flow equations for each fluid phase are written in terms of fluid phase pressures and saturations. These equations are coupled through the moisture retention function, which relates the contrast between fluid phase pressures to the fluid saturations. The difference in phase pressures is defined as the capillary pressure:

$$P_c \equiv P^n - P^w \quad (1)$$

where

- $P_c$  capillary pressure (macroscopic), equal to  $f(S^w$  or  $S^n)$ ;
- $P^\alpha$  pressure of fluid phase  $\alpha$ ,  $\alpha = w, n$ ;
- $S^\alpha$  saturation of fluid phase  $\alpha$ ,  $\alpha = w, n$ ;
- $w, n$  wetting and nonwetting fluid phases, respectively.

The relative permeability-saturation ( $k_{r,\alpha}$ - $S^\alpha$ ) function is required for the parameterization of the generalized form of Darcy's law. The common parameter, saturation, serves to link the two constitutive relationships and provides further coupling of the flow equations through the additional constraint that the fluid saturations sum to unity.

Multiphase transport models, in turn, are coupled to the flow equations through the volumetric flux and are thus indirectly linked to the constitutive relations. Most phenomenological models for the description of residual NAPL dissolution are based on a parameterization relating the mass flux of dissolving NAPL to the interfacial area between fluid phases, a mass transfer coefficient, and the concentration difference across the fluid-fluid interface [e.g., *Miller et al.*, 1990]. This formulation expresses the concept that mass transfer is governed, in part, by the spatial distribution of the fluids. If the more soluble chemical components are to move directly from the NAPL phase into the aqueous phase, then the fluid-fluid interface separating the fluid phases must be crossed. Thus interfacial area serves as a limiting factor on the dissolution process.

What is common to the multiphase flow and transport problems is that both are heavily dependent on the pore-scale physics of fluid-fluid interfaces. This is stated explicitly in the

phenomenological model for NAPL dissolution, but the connection to the multiphase flow constitutive relationships is implicit at best. Both the  $P_c$ - $S^\alpha$  and  $k_{r,\alpha}$ - $S^\alpha$  relationships are nonlinear and hysteretic. Their complex functional form results from the aggregation of many pore-scale physical processes. These include fluid-solid interactions and properties such as wettability and contact angle hysteresis, the effects of pore geometry, fluid properties, and fluid-fluid interactions [see, e.g., *Bear*, 1972; *Dullien*, 1992; *Hillel*, 1982]. These also include the pore-scale processes associated with the movement of fluid-fluid interfaces, primarily through the irreversibility of drainage and imbibition displacement events at the pore scale. These interfaces can support nonzero stresses and thus allow pressure differences to exist between the fluid phases. The shape and movement of the interfaces captures much of the physical interaction between the fluids and between the fluids and solid. Fluid-fluid interfaces also serve as internal system boundaries. If flow is to take place, then the interfaces must move or the flow must be constrained within these internal boundaries. If saturation is to change, then these boundaries must move. In a sense, the distinguishing feature of multiphase systems is the existence of fluid-fluid interfaces [*Gray and Hassanizadeh*, 1991a].

Recently, *Hassanizadeh and Gray* [1993a, b, 1990] have developed a theory that explicitly incorporates the physics of phase interfaces into the governing flow equations. Their theory is based on careful volume averaging from the pore scale to the porous medium continuum scale. At the continuum scale, interfacial area per unit volume of porous medium becomes an independent variable, and a new, thermodynamically based definition of capillary pressure is hypothesized. Their definition of capillary pressure includes increased functional dependence on the interfacial area per unit volume between all phases in the system [*Hassanizadeh and Gray*, 1990]. Of primary interest to NAPL dissolution problems is the proposed functional dependence of  $P_c$  on  $a^{wn}$ , the interfacial area per unit volume of wetting and nonwetting phases. This is a somewhat radical departure from the more simple functional dependence of the traditional theory. The implication is that the standard definition of capillary pressure results in a hysteretic moisture retention function as a result of its incomplete functional dependencies. *Hassanizadeh and Gray* [1993a] reason that the hysteretic moisture retention function is an artifact of projecting the  $P_c$ - $S^w$ - $a^{wn}$  surface onto the  $P_c$ - $S^w$  plane. (See *Hassanizadeh and Gray* [1993a, b, 1990] and *Gray and Hassanizadeh* [1991a, 1991b] for details).

Quasi-static network models provide a unique means of testing for a functional dependence of capillary pressure on interfacial area by providing a systematic bridge between the microscopic and macroscopic scales. Numerical simulations may be set up to mimic physical experiments used to measure the moisture retention function for soil or rock cores. A three-dimensional network of pores with external connections to wetting and nonwetting fluid reservoirs serves as a computational porous medium (see Figure 1). The displacement of the fluids is then governed by the stability of menisci within the network. A capillary pressure is imposed on the system, and each meniscus is interrogated for stability using the Young-Laplace equation, which relates the equilibrium meniscus geometry in a cylindrical capillary tube to the capillary pressure, surface tension, and contact angle:

$$P_c = \frac{2\sigma^{wn} \cos \theta}{R_{\text{eff}}} \quad (2)$$

where

- $P_c$  capillary pressure (microscopic);
- $R_{\text{eff}}$  effective radius of the top of the meniscus;
- $\sigma^{wn}$  surface tension between wetting and nonwetting fluid phases;
- $\theta$  contact angle.

Unstable menisci result in the displacement of one fluid by another. Displacement continues until all menisci are found to be stable. Details of these calculations are given in the following section.

The resultant macroscopic properties of the system, i.e., the fluid saturations and the interfacial area between fluids, may then be calculated using the equilibrium fluid configuration. Fluid saturations are calculated by summing the actual fluid volumes within the pores and dividing by the volume of the pore network. The interfacial area between fluid phases per unit volume of porous medium is calculated by summing the areas of all menisci and dividing by the total volume of the system, including the solid phase volume. These calculations require complete knowledge of the geometry of all menisci. This is facilitated by the use of a highly structured network of pores. Traditionally, network models have involved pore elements having simple geometric shapes arranged on a regular lattice. If the cross sections of the pore elements are circular, then the actual radius of a meniscus is equal to its effective radius, and so its geometry is fully constrained.

Fortunately, the hypothesized definition of capillary pressure of Hassanizadeh and Gray can be shown to reduce to the traditional definition of capillary pressure, equation (1), at equilibrium [Hassanizadeh and Gray, 1990]. Because, in the network model, the system properties are determined only at equilibrium, the standard definition of capillary pressure, (1), may be used. The macroscopic capillary pressure may then be taken as the difference between the nonwetting and wetting fluid reservoir pressures, as in physical experiments. The movement and deformation of the individual fluid-fluid interfaces, however, is governed by the microscopic capillary pressure at the locality of the meniscus. Fluid regions that have become isolated from their respective reservoirs can have pressures that are unrelated to the current reservoir pressures. These pressures are recorded as the simulation progresses. The local

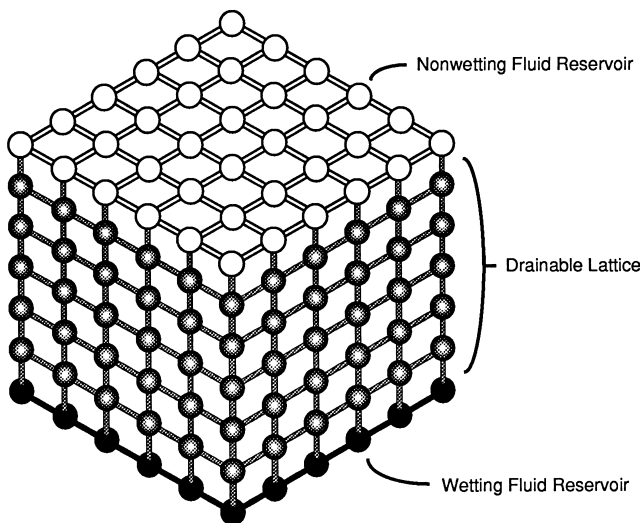


Figure 1. Cubic pore network.

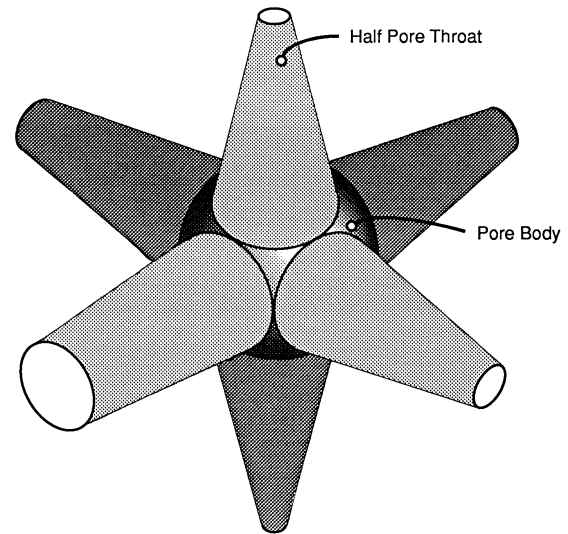


Figure 2. Typical spherical pore body with its associated biconical pore throats.

fluid pressures are used to define the microscopic capillary pressure for use with the Young-Laplace equation (2).

### Network Model Formulation

The network model developed for this study uses a quasi-static displacement process such as that described above and is similar to those developed by, for example, Soll [1991], Jerauld and Salter [1990], and Ferrand and Celia [1989]. The pore space network is three dimensional, and two immiscible fluid phases are simulated. The model is capable of simulating both drainage and imbibition.

### Pore Space Geometry

The pore network simulated in the model is a cubic lattice with constant node spacing. Thus the nodes of the lattice, or pore bodies, have six orthogonal connections to their neighbors (see Figures 1 and 2). These connections are often referred to as pore throats. The top of the lattice serves as a reservoir for nonwetting fluid, while the bottom serves as the wetting fluid reservoir. The four lateral sides of the pore network have no further connections and act as “no-flow” boundaries.

The elements of the pore network consist of two simple geometric shapes. The pore bodies are represented by spheres, as have been used by most past researchers. The pore throats are biconical tubes with the constriction located at the midpoint between pore body centers (see Figures 2 and 4). The radius of the biconical sections at the point of attachment to the pore body is fixed at  $r_b/\sqrt{2}$ , where  $r_b$  is the pore body radius. This creates a well-defined pore space and ensures that menisci cannot overlap one another. It also approximates the converging-diverging character of the pore space of real porous media. This geometry has been used by Nowicki *et al.* [1992], among others, and differs from the traditional, cylindrical connection used by most other researchers. Cylindrical pore throats force the location of fluid-fluid interfaces to be restricted to the connection between the pore body and pore throat; a biconical pore throat allows for a greater range of menisci locations because they may reside within the pore throat as well as at the pore body-pore throat connection and the pore throat constriction. It should be noted that this pore

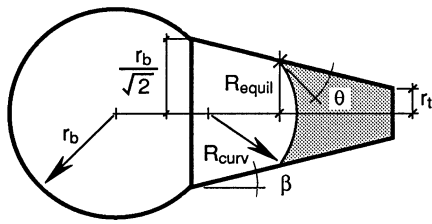


**Figure 3.** Meniscus geometry in a conical capillary of circular cross section.

space representation does not possess “corners” where pendular fluid could reside, as would exist in real porous media with grain to grain contact points. The proposed fluid displacement rules used in the model address this shortcoming in a limited way.

### Lattice Construction

A realization of the pore space is constructed by assigning radii to the lattice elements using a beta probability distribution. The beta distribution is attractive due to its flexibility and the fact that it has fixed upper and lower bounds. A minimum lower bound of zero is an obvious constraint, while an upper bound approaching the half spacing of the lattice is desired to prevent the overlap of pore bodies. This distribution has been widely used in simulations of consolidated rocks and monodisperse spheres [Jerauld and Salter, 1990; Chatzis and Dullien, 1982; Payatakes *et al.*, 1980]. The pore body constriction radii and pore throat constriction radii are generated independently. Following the radii assignments, the pore throats are checked against their adjacent pore bodies, and any that are found to be greater than  $r_b/\sqrt{2}$ , where  $r_b$  is the radius of the smaller of the adjacent pore bodies, are redefined to a value of  $r_b/\sqrt{2}$ . While this introduces a degree of correlation between the pore throat radii and the pore body radii, its effect can be mitigated by specifying probability density functions for the pore throats and pore bodies that are nonoverlapping. If desired, the spacing between pore body centers can then be varied in order to adjust the overall porosity of the system.

### Fluid Displacement Procedure

Displacement of one fluid by another rests upon the definition of fluid regions as “free” or “trapped.” Only free fluids are available for potential displacement. Free fluid regions are those that have a continuous path back to their respective reservoirs, while trapped regions of fluids have become isolated. Additionally, isolated wetting fluid may be defined as free in order to simulate a strongly wet system; in this case a wetting film may be seen as connecting the isolated wetting fluid regions to their reservoir. The existence of continuous wetting films allows a zero residual wetting phase saturation to be achieved, as observed in physical experiments involving strongly wet systems [Dullien *et al.*, 1986]. The identification of free and trapped fluid regions is performed at the end of each capillary pressure step. Any free fluid may be displaced at the subsequent capillary pressure step. In addition, the capillary pressure value of the most recent displacement step is recorded for all the newly trapped fluid regions. This is done so that the menisci of trapped regions can be “frozen” into position to ensure that the volumes of the trapped regions can be maintained at subsequent capillary pressure values.

Displacement takes place along the composite interface composed of all the menisci separating free fluid phases. The individual menisci are interrogated in turn at the given, local,

capillary pressure, and fluids displace each other when a meniscus is found to be unstable. A special version of the Young-Laplace equation for a conical capillary is used to check for meniscus stability [Dullien, 1992, p. 192] (See Figure 3):

$$R_{\text{equil}} = \frac{2\sigma^{wn}|\cos(\theta + \beta)|}{P_c} \quad (3)$$

where

- $P_c$  capillary pressure (microscopic);
- $\sigma^{wn}$  surface tension between wetting and nonwetting fluid phases;
- $\theta$  contact angle;
- $\beta$  half angle of the cone;
- $R_{\text{equil}}$  equilibrium radius of the top of the meniscus.

In this manner the composite interface is gradually deformed from its initial configuration. When all the menisci along the composite interface are found to be stable, the system has reached a new equilibrium.

**Drainage mechanisms.** Nonwetting fluid may displace wetting fluid via two mechanisms. The primary mechanism is governed by the constriction radii of the pore throats. Equation (3) is used to examine the stability of interfaces within the pore throats in the limiting case of  $\beta = 0^\circ$ , corresponding to the constriction where the sides of the capillary are parallel (see Figures 3 and 5). If the constriction radius is too large, then a “Haines jump” occurs [Haines, 1930], and the nonwetting fluid invades the pore throat. The adjacent pore body will also drain because its size will be larger than the pore throat. This mechanism, often referred to as “piston drainage,” is the standard drainage rule used by most network modelers [e.g., Soll, 1991; Jerauld and Salter, 1990; Ferrand and Celia, 1989].

A secondary mechanism for drainage is invoked if a “singlet” of wetting fluid is left stranded between drained pore bodies during the displacement procedure. When this occurs, the locations of the menisci at either end of the singlet are explicitly calculated to test whether or not they intersect. If they are found to intersect, then the wetting fluid within the pore throat is displaced by nonwetting fluid. The details of the meniscus location calculations are the same as those listed below in the saturation and interfacial area calculation discussion. This mechanism is unique to network models involving biconical pore throats. It is not strictly rigorous in addressing the stability of fluid membranes but captures the behavior presented by Toledo *et al.*, [1994]. It serves to prevent the buildup of wetting fluid singlets which, if left in place, cause excessive trapping of nonwetting fluid and result in significant trap hysteresis [Blunt *et al.*, 1992; Wardlaw and McKellar, 1981]. Micromodel studies indicate that isolated singlets of wetting fluid are more readily displaced than larger regions of fluid, although this effect is facilitated by pendular fluids [Soll, 1991, p. 192]. The inclusion

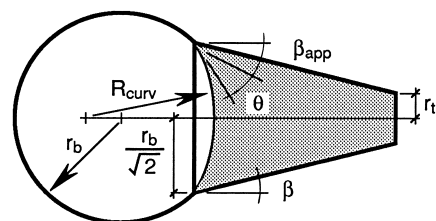


**Figure 4.** Meniscus geometry at the pore body-pore throat contact.

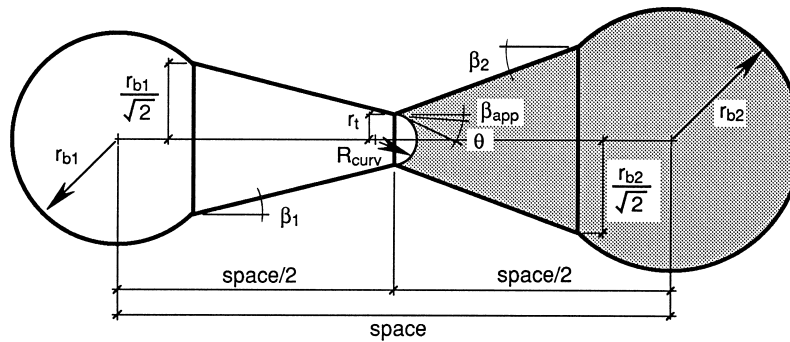


Figure 5. Meniscus geometry at the pore throat constriction.

of this secondary drainage mechanism serves to capture, in a simplified way, this physical behavior.

**Imbibition mechanisms.** The displacement of nonwetting fluid by wetting fluid is governed by the pore body radii. As with drainage, equation (3) is used to test whether or not a meniscus can span a pore body. The half cone angle  $\beta$  is set to zero, which corresponds to the hemisphere of the pore body where the sides are parallel. If spanning is possible, then the wetting fluid invades the pore body and its surrounding pore throats, since the pore throats are always smaller than the pore body. This mechanism, referred to as “piston displacement” or “retraction,” is the simplest form of the standard imbibition rule. More involved displacement formulations based on local fluid configurations in the vicinity of the meniscus [Blunt *et al.*, 1992; Jerauld and Salter, 1990] are not included for simplicity. As well, no “snap-off” mechanisms are simulated in the model, again for simplicity. Snap-off is enhanced by the presence of pendular fluid which is lacking in the current pore geometry [Li and Wardlaw, 1986a, b; Lenormand and Zircon, 1984]. As well, this mechanism is somewhat dependent on the shape of the pore bodies [Mohanty *et al.*, 1987], which makes the formulation of a snap-off displacement rule somewhat arbitrary. To facilitate the interpretation of the model results, no snap-off mechanisms are included in the model.

### Saturation and Interfacial Area Calculations

The actual locations of menisci separating fluid phases are not specifically calculated during the displacement procedure except when isolated singlets of wetting fluid are examined. Instead, they are only tracked in a cursory sense so that they are known to be located within a particular pore throat. In order for the saturation and interfacial area calculations to be performed, the location and geometry of all the fluid-fluid interfaces must be calculated explicitly. This requires the calculation the equilibrium radius and radius of curvature for each meniscus. The equilibrium radius is calculated using the Young-Laplace equation (3). The radius of curvature may then be calculated using the equilibrium radius, the contact angle, and the half angle of the conical capillary. These are related by [Dullien, 1992, p. 192] (see Figure 3)

$$R_{\text{curv}} = \frac{R_{\text{equil}}}{|\cos(\theta + \beta)|} \quad (4)$$

where  $R_{\text{curv}}$  is the radius of curvature of the meniscus.

Once these values are calculated, the boundaries separating solid and fluid phases are known. Fluid saturations are calculated by summing the volumes of simple geometric shapes (truncated cones, spherical caps, and spheres) and dividing by

the total pore volume. Although pendular films were assumed to exist to facilitate the displacement of isolated wetting fluid, the volumes of these films are considered negligible and do not contribute to the saturation calculations. The interfacial area between fluid phases consists of a summation of the area of spherical caps formed by the menisci. The total interfacial area is then divided by the total volume of the averaging volume, including the volume occupied by the solid, to arrive at the interfacial area between fluid phases per unit volume of porous medium,  $a^{wn}$ . The interfacial area contributed by films is not included in the calculation of  $a^{wn}$ . In this manner, only those fluid-fluid interfaces whose curvature is governed by the capillary pressure contribute to the interfacial area. This definition differs from traditional equilibrium thermodynamic definitions of  $a^{wn}$  but appears to be consistent with the theory of Hasanizadeh and Gray [1990].

A meniscus may be located at three general positions: somewhere within a pore throat, at the entrance to the adjacent pore body, or at the pore throat constriction (See Figures 3, 4, and 5 respectively). If the equilibrium radius of the meniscus is found to be located within the pore throat, then (3) and (4) apply. During imbibition the calculated equilibrium radius of a meniscus may be found to be larger than the radius of attachment of the pore throat to the pore body but still too small to have spanned the pore body and caused imbibition displacement. In this case, (3) is inverted and an apparent cone angle  $\beta_{\text{app}}$  is determined using a fixed equilibrium radius of  $r_b/\sqrt{2}$ . A new radius of curvature can then be found using (4) and  $\beta_{\text{app}}$ . This procedure mimics a geometrically smooth transition at the attachment between the pore throat and the pore body rather than a sharp corner. A similar situation may arise during drainage when the equilibrium radius of a meniscus may be found to be smaller than the pore throat constriction though drainage displacement has not occurred. This is possible because the limiting condition for displacement during drainage is  $\beta_{\text{app}} = 0^\circ$ . In this situation the equilibrium radius of the meniscus is fixed at the bond constriction radius, and (3) is used to solve for an apparent cone angle. A radius of curvature is then calculated using (4) as in the previous situation. Again, this is equivalent to a geometrically smooth transition at the pore throat constriction.

## Results and Discussion

### Representative Elementary Volume Determination

Fluid saturations and interfacial areas per unit volume are properties that are poorly defined at the pore scale. Volume averaging must be invoked in order to define these quantities

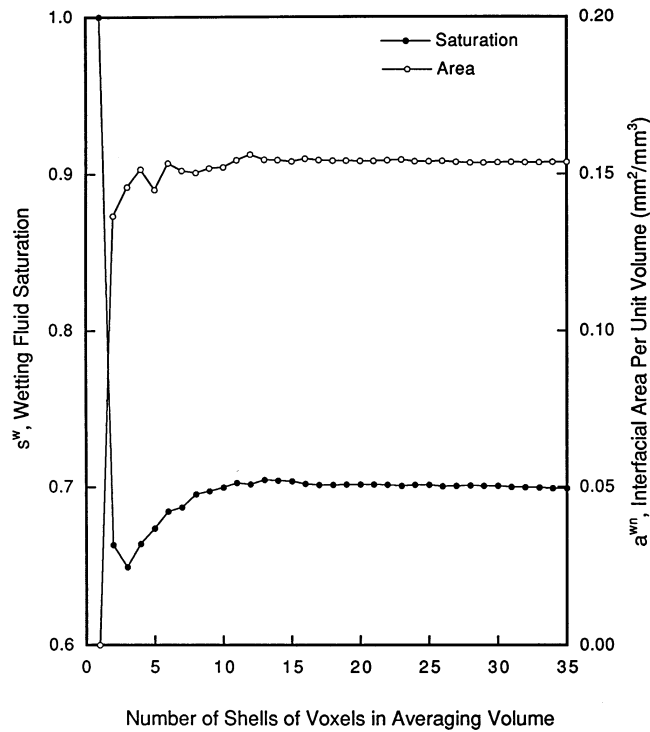


Figure 6. Representative elementary volume results.

at the continuum scale. The averaging must be performed at a volume sufficiently large that the resulting fields are smooth, well defined, and insensitive to changes in the averaging volume. Such a volume is referred to as a representative elementary volume, or REV [Bear, 1972, pp. 19–20].

An REV for the network model simulation was determined by analyzing the wetting fluid saturation and interfacial area per unit volume for a range of subvolumes within the pore lattice. The smallest volume consisted of the central pore body and its six adjacent half pore throats, often referred to as a voxel (See Figure 2). The second volume consisted of the central voxel and the shell of voxels surrounding it. The volumes were increased by adding shells of voxels until the entire lattice was included in the calculations. Figure 6 shows the results of this test for the wetting fluid saturation and the interfacial area between fluid phases. The quantities, as expected, are seen to be erratic for small averaging volumes but approach a limiting behavior above approximately 17 shells. The values can be seen to diverge slightly from this limiting behavior as the influence of the boundaries is felt. This behavior is consistent with results reported by Ferrand and Celia [1992a]. The wetting fluid saturation and the interfacial area can also be seen to reach their limiting behaviors at the same volume. Investigation of the averaging behavior over a broad range of saturation values shows that the REV size is independent of the saturation at which the simulation is performed. On the basis of these results, an REV value of  $40^3$  pore bodies was chosen (corresponding to  $1728 \text{ mm}^3$  at the given node spacing). The subsequent simulation was performed using a lattice of  $50^3$  pore bodies, and the five outer shells were omitted from the saturation and interfacial area calculations to minimize boundary effects.

### Moisture Retention Function Simulation

In order to investigate the hypothesis concerning the functional relationship between capillary pressure, saturation, and

interfacial area, a displacement simulation was performed using a series of 3989 sequential capillary pressure steps. Fluid saturation and interfacial area calculations were performed at the end of each displacement step. The simulation was designed to provide saturation and interfacial area values both on and within the main hysteresis loop, such that complete sets of imbibition and drainage scanning curves were calculated. Details of the input parameters for the simulation are provided in the appendix; these parameters correspond to an air-water system that is strongly water wet.

**Primary drainage and main hysteresis loop.** The simulation was begun under fully saturated conditions; the lattice was then drained to zero residual over 60 capillary pressure steps. This was followed by a main imbibition cycle of 50 steps where the wetting fluid saturation reached a maximum value of 74.4%. At this point the only nonwetting fluid remaining in the lattice was trapped. The main hysteresis loop was then defined by another cycle of main drainage followed by main imbibition using the same capillary pressure step sequences.

The moisture retention function resulting from these steps is plotted in Figure 7a. The primary drainage curve can be seen to be separated from the main hysteresis loop and shows a distinct entry pressure of 50 cm  $\text{H}_2\text{O}$ . The main hysteresis loop is repeatable and shows a very abrupt decrease in saturation at an entry pressure of about 41 cm  $\text{H}_2\text{O}$ . This is a noticeably lower entry pressure than for primary drainage. The reduced entry pressure and the resulting sharp break in saturation during main drainage are caused by the presence of trapped nonwetting phase regions. The trapped regions aid in the propagation of nonwetting fluid pathways through the lattice by increasing the number of individual menisci along the invasion front and thus increasing the probability of fluid displacement. This accentuates the break in saturation during main drainage and accounts for the decreased entry pressure.

Figure 7b shows a plot of wetting fluid saturation versus interfacial area per unit volume for the same sequence of capillary pressure steps. The endpoints of the primary drainage curve represent single-phase systems, and thus the interfacial area values are zero. The sudden increase in interfacial area at the high end of the saturation range corresponds to the entry pressure of the primary drainage curve of the moisture retention function. The primary drainage curve is asymmetric about the saturation axis with a maximum value of  $0.267 \text{ mm}^2/\text{mm}^3$  at a wetting fluid saturation of 27.1%. The steep decrease in interfacial area as the primary drainage curve approaches 0% saturation represents the loss of the menisci contributed by isolated singlets as they are finally drained.

The saturation–interfacial area relationship is seen to be hysteretic for the data points corresponding to the main hysteresis loop in the moisture retention function and its crescent shape is similar to that hypothesized by Hassanzadeh and Gray [1993a, Figure 8]. During the main imbibition cycle the interfacial area can be seen to increase to its maximum value at a saturation of 38.1%, just after crossing the primary drainage curve. The interfacial area then decreases in a symmetric fashion before leveling off as residual nonwetting phase saturation is achieved. The main drainage curve is similar in shape to the main imbibition curve but has higher interfacial area values throughout its range and reaches its maximum at a lower saturation value. At the beginning of the main drainage sequence the interfacial area and saturation values remain constant for the capillary pressure values below the entry pressure. This, again, is the result of the trapped nonwetting fluid regions. The fluid–fluid interfaces surrounding these regions ac-

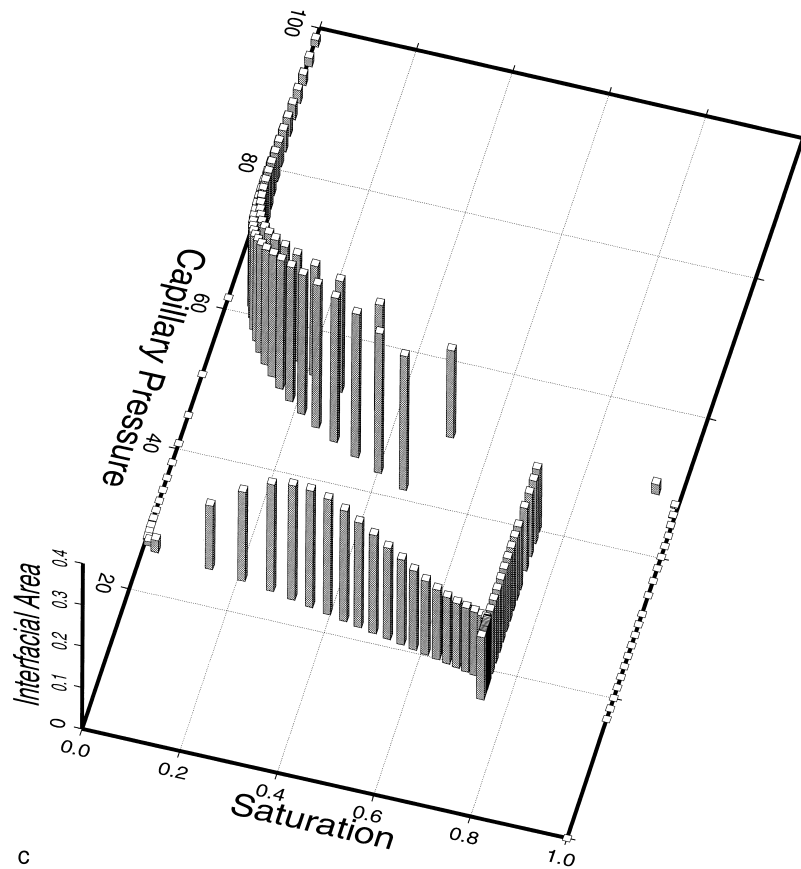
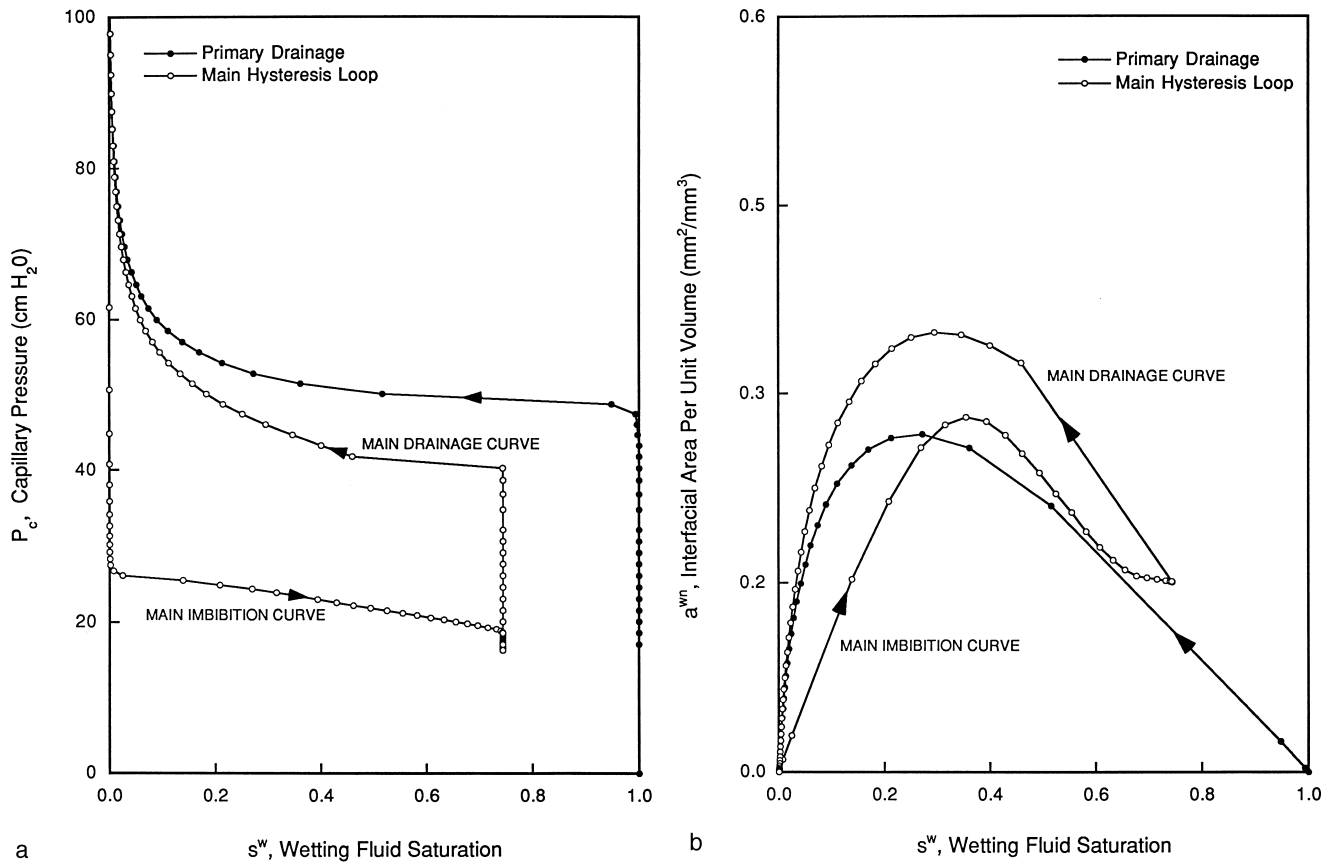


**Figure 7.** Primary drainage and main hysteresis loop: (a) capillary pressure versus saturation, (b) interfacial area versus saturation, and (c) capillary pressure versus saturation versus interfacial area.

count for all the net interfacial area at this point in the simulation. They are not allowed to deform so as to preserve their volumes. This causes the saturation and interfacial area to be fixed prior to reaching the entry pressure during the subsequent drainage cycle. An abrupt increase in interfacial area follows and reaches a maximum value of  $0.348 \text{ mm}^2/\text{mm}^3$  near a saturation of 29.5%. The interfacial area then decreases smoothly to zero as drainage is completed.

The complex shape of the main hysteresis loop results from several pore-scale events that take place as the menisci separating fluid phases adjust to new capillary pressure conditions. The adjustments may involve Haines jumps (fluid displacement) [Haines, 1930] or movement of individual menisci within their original pore throat (meniscus adjustments). Fluid displacements may result in the “spawning” of new menisci or the destruction of old menisci, depending on the local fluid configurations. The adjustment of menisci within a pore throat and the stranding of a meniscus at the pore throat constriction or pore throat–pore body contact will also produce changes in its interfacial area. The proportion of displacement to adjustment events depends on the local fluid configuration, which, in turn, depends on the overall saturation state of the lattice. As a result, certain events will dominate over specific ranges of saturation. It should also be noted that both types of events can produce increases or decreases in interfacial area during both drainage and imbibition. Despite the complexity of these pore-scale processes, the net result is a smooth functional relationship between capillary pressure and saturation throughout the main hysteresis loop.

Figure 7c shows a three-dimensional plot of the moisture retention function using the additional axis of interfacial area. The vertical axis is interfacial area per unit volume of porous medium, and the origin of the plot lies at the lower left-hand corner. The combination of the two, two-dimensional plots yields a well-behaved main hysteresis loop in three-dimensional space. The points of maximum interfacial area are clearly visible on all three curves, with the highest value corresponding to the main drainage curve. The constant saturation and interfacial area values corresponding to the first few capillary pressure steps of the main drainage curve also stand out. This figure is similar to the results Gvirtzman and Roberts [1991] obtained in their investigation of the interfacial area associated with pendular wetting fluid in sphere packs.

**Drainage scanning curves.** After defining the main hysteresis loop, a series of drainage scanning curves were generated to investigate the interfacial area behavior interior to the loop. The capillary pressure sequence for the drainage scanning cycles was constructed by first imbibing through a series of pressure steps derived from the original master list for imbibition. The imbibition sequence was stopped prior to reaching the residual nonwetting phase saturation at an intermediate capillary pressure value. The drainage scanning curve was then generated by subsequent drainage to zero residual wetting phase saturation. The drainage steps were derived from the master list of capillary pressure steps for drainage and included only those capillary pressure values higher than the final imbibition step. The subsequent drainage scanning curve sequence included two more imbibition steps. In this manner, 15 drainage scanning curves were generated.

The moisture retention function including the drainage scanning curves is shown in Figure 8a. The primary drainage curve has been omitted for clarity, and one of the scanning curves has been highlighted. The behavior is similar to that

seen in physical measurements with the scanning curves lying completely within the main hysteresis loop. The curves do not cross one another, and they mirror the shape of the main drainage curve. The drainage scanning curves originating from the vicinity of the residual nonwetting fluid saturation begin to mimic the shape of the main drainage curve. All scanning curves converge to a point at zero residual wetting phase saturation. The first few steps of each drainage curve represent capillary pressure values that are too low to cause a Haines jump (i.e., piston displacement) anywhere in the lattice, and hence the decrease in saturation results solely from the movement of menisci within their pore throats. The drainage scanning curves originating from the flat portion of the main imbibition curve have as much as 20% saturation decreases due solely to this mechanism.

The corresponding saturation and interfacial area values are plotted in Figure 8b. The same drainage scanning curve has been highlighted as in Figure 8a and again, the primary drainage curve has been omitted. The scanning curves can be seen to originate from the main imbibition curve and then rise sharply in interfacial area. All but the first two scanning curves cross the main drainage curve as they do so. After reaching their maximum values, the interfacial areas decrease abruptly. As the scanning curves approach the main drainage curve, they become asymptotic to it. They then follow the main drainage curve to the origin. The scanning curves with the largest maxima are those that depart from the flat portion of the main imbibition curve of the moisture retention function. The set of drainage scanning curves can be seen to be bounded by an upper envelope that mirrors their individual shape. The envelope maximum in interfacial area is about  $0.57 \text{ mm}^2/\text{mm}^3$  and occurs just below 50% wetting fluid saturation.

The three-dimensional plot of these two figures is shown in Figure 8c. Again, the primary drainage curve has been omitted, and the same drainage scanning curve has been highlighted. The set of drainage curves can be seen to form a unique, though complex, surface in three-dimensional space. The maximum value of the surface is located within the main hysteresis loop and corresponds to the maximum in the bounding envelope of Figure 8b. The surface has curvature in all directions and appears to be smooth and well behaved. The major axis of the surface, or hinge line, corresponds to the bounding envelope of maximum interfacial area seen in Figure 8b.

**Imbibition scanning curves.** Imbibition scanning curves were calculated following the drainage scanning curve sequence. The capillary pressure steps for the imbibition scanning curves were generated in a similar manner to those used to generate the drainage scanning curves. The lattice was first drained from the residual nonwetting phase saturation through a series of capillary pressure steps derived from the original master list of 60 drainage steps. Drainage was stopped at an intermediate point and then followed by imbibition. The imbibition steps were taken from the master list of the imbibition set and included those capillary pressure values lower than the final intermediate drainage step. Subsequent imbibition scanning curves followed in the same manner but with two additional drainage steps each time. A total of 22 imbibition scanning curves were generated.

The moisture retention function showing the imbibition scanning curves is plotted in Figure 9a. Again, the primary drainage curve has been omitted, and one scanning curve has been highlighted. The imbibition scanning curves can be seen to mirror the shape of the main imbibition curve. Those orig-

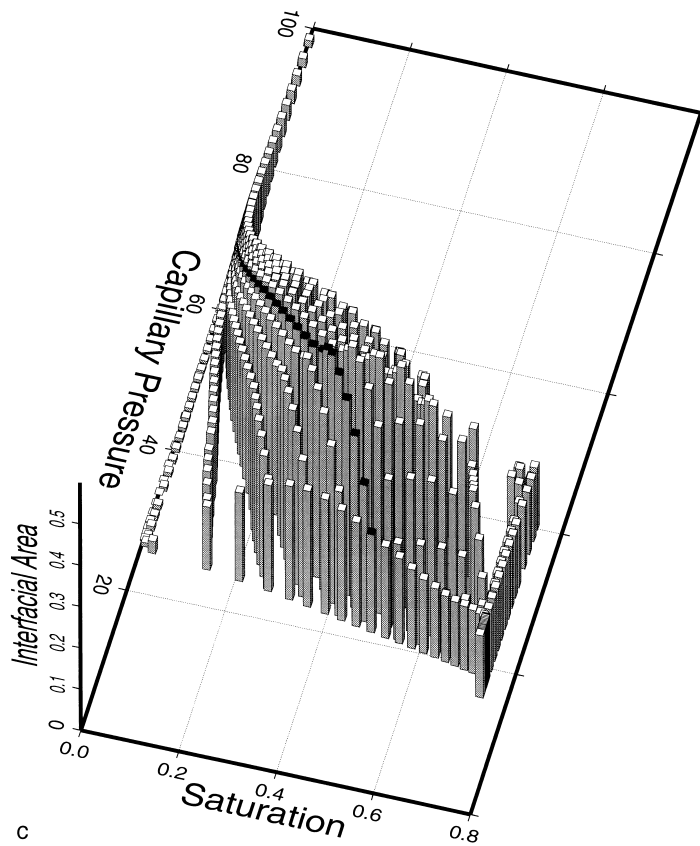
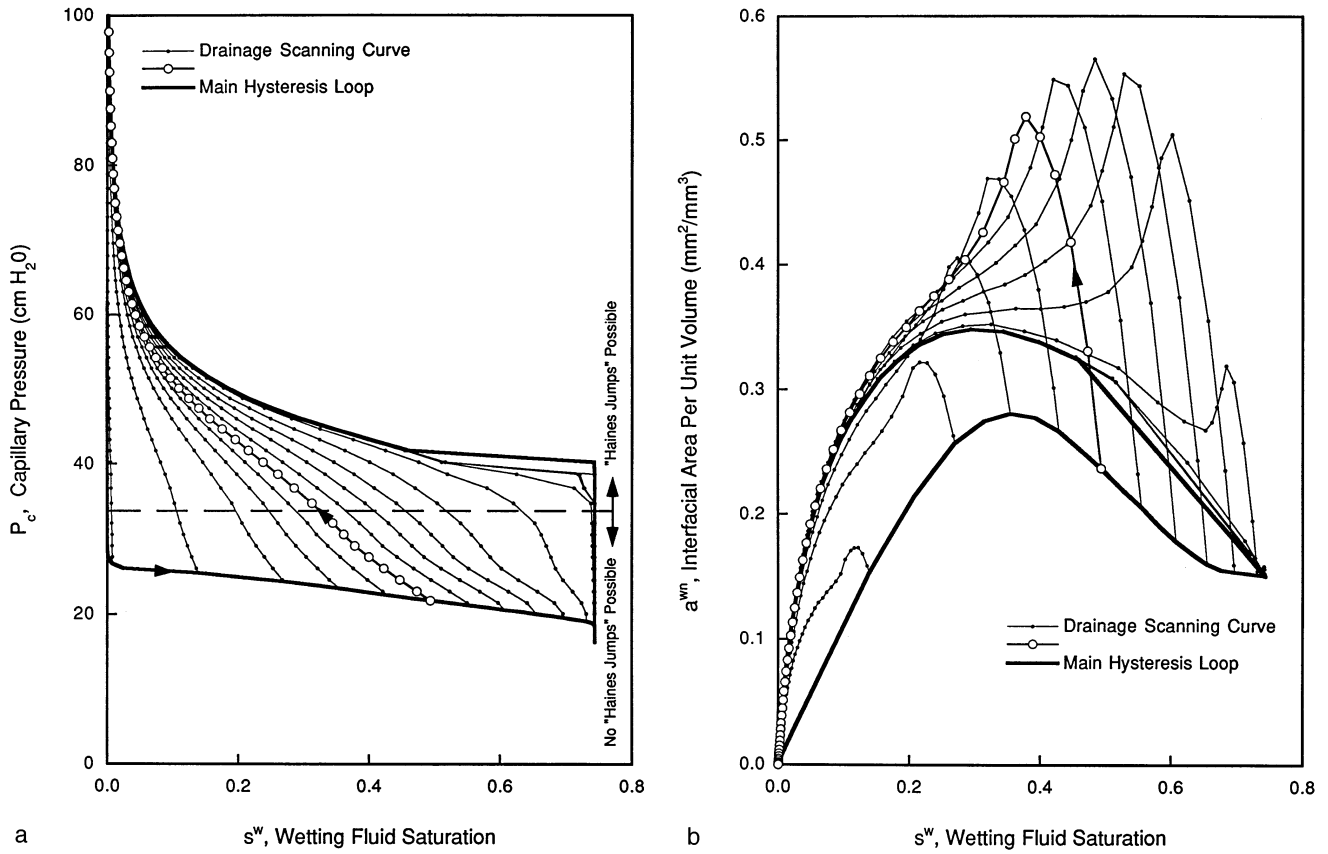


Figure 8. Main hysteresis loop and drainage scanning curves: (a) capillary pressure versus saturation, (b) interfacial area versus saturation, and (c) capillary pressure versus saturation versus interfacial area.

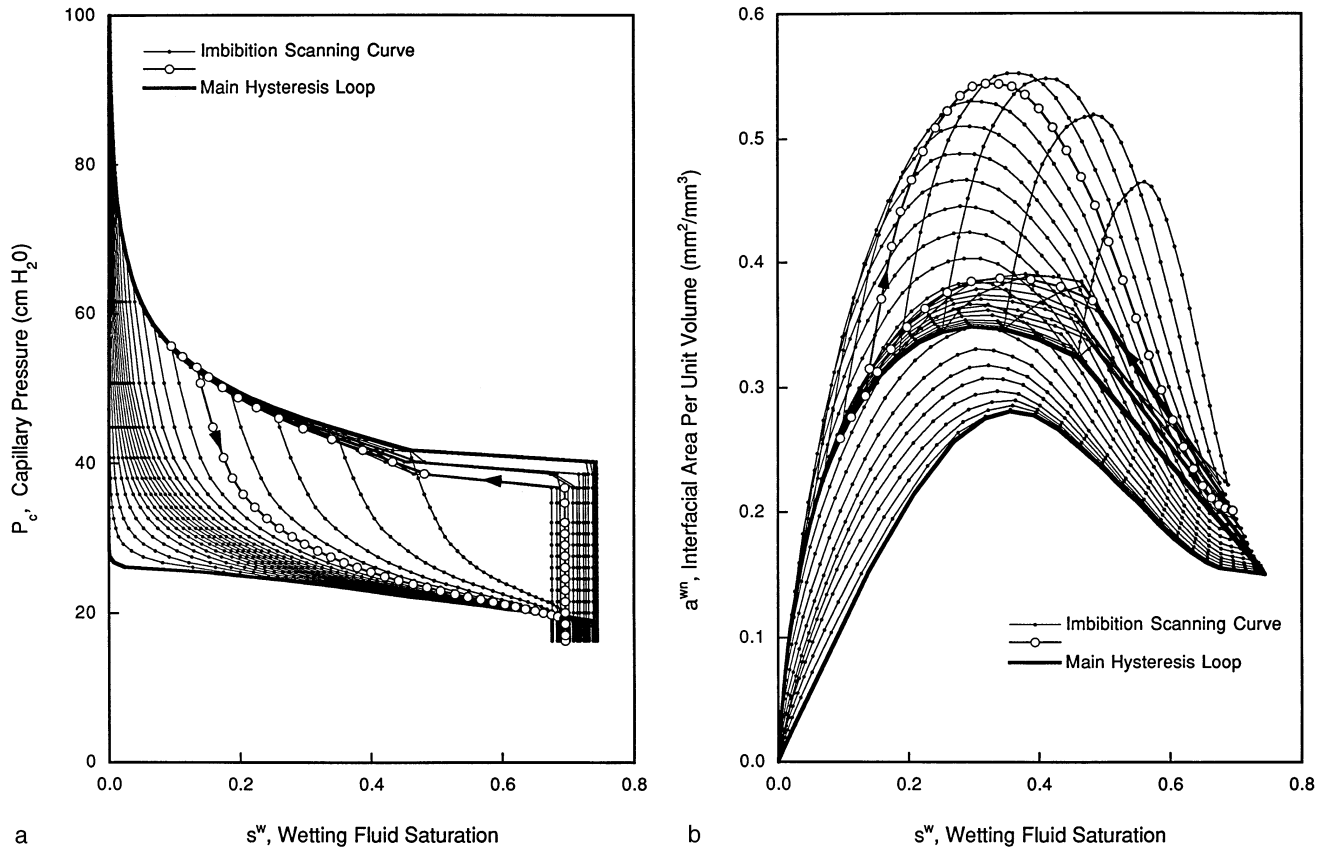


Figure 9. Main hysteresis loop and imbibition scanning curves: (a) capillary pressure versus saturation, (b) interfacial area versus saturation, and (c) capillary pressure versus saturation versus interfacial area.

inating at lower capillary pressure values show a much more gradual curvature than those closer to the main imbibition curve. There is also a “trap hysteresis” associated with the imbibition scanning curves. Trap hysteresis is the lowering of the final wetting fluid saturation that can be obtained during imbibition. This phenomenon results from the additional trapping of nonwetting fluid regions caused when the lattice is not completely drained prior to imbibition. The subsequent drainage sequence is thus slightly different from the main drainage curve. The most extreme case seen in Figure 9a has an 8% final saturation reduction. This corresponds to the first scanning curve, which originates at the drainage step just following the entry pressure. The trapping behavior becomes less pronounced as the imbibition scanning curves originate at higher capillary pressure values on the main drainage curve. This phenomenon has been documented in physical experiments and is discussed in depth by *Wardlaw and McKeller* [1981].

The same set of data points is plotted on the saturation–interfacial area plane in Figure 9b. The imbibition scanning curves originate from the main drainage curve or the intermediate drainage curves that result from the trap hysteresis. Like the drainage scanning curves, the change in interfacial area along the imbibition scanning curves is not monotonic. Unlike the drainage scanning curves, the maximum values reached by the individual imbibition scanning curves do not occur at sequential saturation values. Instead, the first nine scanning curves have their peaks at sequentially lower saturation values, while the remaining curves have their maxima at sequentially higher saturation values. The first four scanning curves are relatively symmetric and reach successively higher maximum values. The remainder of the curves have successively lower maximum interfacial area values and slowly approach the shape of the main imbibition curve. The final imbibition scanning curve is nearly identical to the main imbibition curve. The trap hysteresis is manifested as the sequence of points forming an irregular line at the far right of the plot above the point of the main hysteresis “crescent.” The intermediate drainage curves that arise from the trap hysteresis can be seen just above the main drainage curve. As in Figure 8b, the maximum interfacial areas achieved by the imbibition scanning curves appear to be bounded. The bounding envelope is very symmetric with a maximum interfacial area value of  $0.56 \text{ mm}^2/\text{mm}^3$  at a saturation value of approximately 37%. The maximum value of the bounding envelope is nearly identical to that of Figure 8b, but the saturation value at which the maximum occurs is significantly lower.

The three-dimensional plot of Figures 9a and 9b is shown in Figure 9c. The shape of the surface is very similar to the surface generated by the drainage scanning curves. It shares the same general curvature and convexity, but there are slight differences with regard to the location of the maximum interfacial area and the curvature orthogonal to the major axis. The region of trap hysteresis significantly affects the shape of the surface. The constant saturation and interfacial area values associated with the drainage steps below the entry pressure result in a planar ramp in the surface at its right edge.

### Discussion of Results

The results of the network model simulation clearly indicate a strong functional dependence of capillary pressure on the interfacial area between fluid phases. This supports the hypothesis of *Hassanizadeh and Gray* [1990]. The surface generated by the drainage scanning curves is slightly different from

that generated by the imbibition scanning curves, but both surfaces share a very similar form (See Figures 8c and 9c). The surfaces have an S-shaped major axis that stretches from the zero residual saturation point, crosses the central portion of the main hysteresis loop, and then terminates at the final point of the main imbibition curve. The main axes, or hinge lines, are represented in the two-dimensional plots of interfacial area versus saturation as upper bounding envelopes for interfacial area (See Figures 8b and 9b). The surfaces have a maximum interfacial area value near the center of the main hysteresis loop and are convex with respect to the capillary pressure–saturation plane. They also appear to be relatively smooth and well behaved.

The curvature displayed by the surfaces suggests that the relationship between capillary pressure, saturation, and interfacial area is very complex. Because of the convex shape of the surface, the functional relationship is not single valued. For any value of capillary pressure there correspond two points on the surface with different saturation values and the same interfacial area. Likewise, for any set value of saturation, there exist at least two different capillary pressure values with the same interfacial area. This may suggest that we should view interfacial area as a function of capillary pressure and saturation, i.e.,  $a^{wn} = f(P_c, S^w)$  rather than  $P_c = f(a^{wn}, S^w)$ . (*M. Hassanizadeh*, personal communication, 1995). It should be noted that these observations are based on the definition of  $a^{wn}$  for which the contributions by wetting films are ignored.

The differences between the surface generated from the drainage scanning curves and the surface generated from the imbibition scanning curves are notable (Figures 8c and 9c). We had hypothesized that these surfaces might match except in systems with contact angle hysteresis. The system modeled used identical contact angles for the advancing wetting fluid, receding wetting fluid, and equilibrium fluid configurations, so contact angle hysteresis cannot account for the differences between the surfaces. The differences could be true manifestations of the complex nature of the constitutive relationship, or they could be artifacts of the simulation method. Possible artifacts include the capillary pressure step sequence used in the simulation and the simplified displacement rules employed.

The sequence in which the scanning curves were generated could be responsible for the differences between the two surfaces. Prior to the generation of the drainage scanning curves, the lattice was completely drained. The drainage scanning curves were then calculated sequentially with one imbibition cycle and one drainage cycle used to generate each scanning curve. The drainage cycles always resulted in complete drainage of the lattice. Because of this procedure the imbibition cycles always began from the same system state, i.e., 0% wetting fluid saturation. As a result, the drainage scanning curves are independent from each other. The same is not true of the imbibition scanning curves, owing to the presence of residual nonwetting phase saturations and trap hysteresis. Because each imbibition scanning curve has a different starting saturation and that saturation is determined as part of a continuous calculation cycle, each imbibition scanning curve is dependent on the entire sequence of capillary pressure steps used for the imbibition scanning curve cycle. This causes the imbibition scanning curves to be dependent on the sequence in which they are generated. Had the imbibition scanning curves been calculated in a different sequence, it is possible that a slightly different surface would have resulted. The capillary pressure step sequence used in the simulation therefore may account for

some of the differences in the surfaces generated from the drainage and imbibition scanning curves.

The simplified imbibition displacement rules would also affect the results of the simulation and thus the shapes of the surfaces. The weakest displacement rule, in a physical sense, is the use of the Young-Laplace equation (3) to test for imbibition displacement. As discussed in the model formulation section, no modifications were made to this rule to account for the local fluid configuration and geometry of the pore body being tested for imbibition. Modifications to this rule, as suggested by other researchers, are somewhat discretionary and typically require the use of an additional fitting parameter [e.g., *Jerauld and Salter*, 1990]. These fitting parameters have only a weak theoretical underpinning and have yet to be physically measured. For these reasons, the most simplistic formulation was used. The other potential fault in the displacement rule formulation involves snap-off mechanisms. No snap-off mechanism was incorporated in the model because the pore space represented in the network model does not account for pendular wetting fluid. Either of these choices concerning displacement rules might account for the differences seen in the surfaces created by the drainage scanning curves and the imbibition scanning curves. The significance of these effects remains to be investigated.

The issue of pendular wetting fluid also arises in comparisons of the pore space simulated by the network model with that of real porous media. The simulated pore space, while possessing connectivity and three-dimensionality, is highly stylized and consists of simple geometric elements with circular cross sections. Real pore spaces, on the other hand, are highly irregular and contain grain-to-grain contact points. These contact points create "corners" in which wetting fluid may reside even after the "core" of the pore space has been invaded by nonwetting fluid. This pendular wetting fluid can contribute significantly to the net saturation and interfacial area of the system. The role played by pendular wetting fluid has been partially examined by *Gvirtzman and Roberts* [1991], who considered the pendular rings associated with packings of perfect spheres. They used the Young-Laplace formulation to calculate the geometry of the fluid-fluid interfaces at a given capillary pressure. This allowed them to calculate the wetting fluid saturation and net interfacial area of the system. Their results are very similar to those seen in Figures 8c and 9c and demonstrate the importance of pendular fluids with regard to saturation and interfacial area. The major limitations of the approach of *Gvirtzman and Roberts* [1991] are that hysteresis cannot be studied and that the interfacial area values corresponding to the intermediate saturation values cannot be determined. These shortcomings are addressed by the network model used in this study.

## Conclusions and Future Research

The results presented in this paper indicate that the interfacial area between fluid phases per volume of porous medium becomes a well-defined macroscopic property at an averaging volume similar to that of saturation. Simulated immiscible displacement experiments were performed to explore how the interfacial area between fluid phases changes during imbibition and drainage in a two-fluid system. The results of the simulations indicate that a functional relationship exists between capillary pressure, saturation, and the interfacial area between fluid phases at the macroscopic scale. The  $P_c$ - $S^w$ - $a^{wn}$  relationship was seen to be consistently smooth and well behaved

throughout a wide range of capillary pressure and saturation values. This implies that direct estimates of fluid-fluid interfacial area could be predicted given information regarding the capillary pressure and saturation of the system under study. This has important implications regarding the prediction of NAPL dissolution and other interfacial mass transfer processes. The smoothness of the simulation results, despite the limitations of the simplified network model used, suggests that this relationship may indeed be fundamental to multiphase systems and provides a measure of verification to the constitutive theory of *Hassanizadeh and Gray* [1990], which hypothesizes such a functional dependence. The nonunique  $P_c$ - $S^w$ - $a^{wn}$  surfaces generated by the drainage and imbibition scanning curve sequences, however, prohibit ascribing the hysteresis seen in the traditional moisture retention function to its being a projection of a simple three-dimensional surface onto the  $P_c$ - $S^w$  plane. The physical causes and implications of this phenomenon remain to be explored.

Further investigation of the  $P_c$ - $S^w$ - $a^{wn}$  relationship using network models should focus on the impact of pendular wetting fluid on both interfacial area and saturation. The pore space simulated by the network model used in this study is too simple to allow the simulation of pendular wetting fluid. It does, however, capture the impact of the "ink bottle" effect that results in the differences between the main drainage and main imbibition curves. An analysis of the role played by pendular wetting fluid will necessitate an improvement in the representation of the pore space but could borrow from the methodology of *Gvirtzman and Roberts* [1991]. Some advances have already been made in this direction. Several researchers have substituted capillary tubes with square or triangular cross sections for the cylindrical pore throats traditionally used in network models [e.g., *Ioannidis and Chatzis*, 1993, *Ioannidis et al.*, 1993; *Chatzis and Dullien*, 1985]. The emphasis, however, has been to study how the hydraulic conductivity of pendular fluids affects relative permeability [e.g., *Ioannidis and Chatzis*, 1993; *Chambers and Radke*, 1991; *Lenormand and Zarcone*, 1984]. These formulations represent a potentially significant advance in our conceptualization of pore space. The significance of wetting fluid films to the interfacial area also remains an unresolved issue. These calculations are performed in the model, but the results were not presented because of space limitations.

A research effort parallel to the computational studies described herein should also be made to measure the interfacial area between fluid phases in real porous media. Experimental results analogous to those given in this paper would further strengthen the hypothesis of *Hassanizadeh and Gray* and provide substantiation of network model results. Physical measurements would also provide a data set with which to calibrate more complex network models. Further improvements in pore space representation, calibration to physical data sets, and improved pendular-fluid-dependent displacement rules (i.e., snap-off) should lead to more realistic network models. Such models should continue to serve as valuable computational tools to investigate a wide variety of multiphase porous media problems.

## Appendix: Network Model Simulation Parameters

### Lattice Geometry

**Input lattice statistics.** The dimensions of the lattice are  $50 \times 50 \times 50$ , and the numbers of pore elements (excluding

**Table A1.** Pore Element Radius Distributions (Beta Distribution)

Lattice Element	Mean, mm	Variance, mm <sup>2</sup>	Minimum, mm	Maximum, mm
<i>Input</i>				
Pore body	0.0650	3.2000E-04	0.0100	0.0900
Pore throat	0.0250	1.3000E-04	0.0100	0.0700
<i>Output</i>				
Pore body	0.0650	3.1991E-04	0.0103	0.0900
Pore throat	0.0229	8.8663E-05	0.0073	0.0588

reservoirs and reservoir connections) are as follows:

Pore bodies	125,000
Pore throats	370,000

Distributions of pore element radii are given in Table A1.

**Output lattice statistics.** Pore throat adjustments are as follows (excluding reservoir connections):

Total	370,000
Total adjusted	74,910

and pore element volumes are (excluding boundary shells)

Pore bodies	58.256 (26.94% of total)
Pore throats	157.970 (73.06% of total)
Total	216.226

Porosity is 12.513%. Distributions of pore element radii are given in Table A1.

### Fluid Parameters

Contact angles (advancing, receding, and equilibrium) are 0.00 rad. Miscellaneous fluid parameters are

Surface tension, dyn/cm	72.00
Wetting fluid viscosity, mPa s	1.00
Wetting fluid density, g/cm <sup>3</sup>	1.00

**Acknowledgments.** This work was supported, in part by the National Science Foundation under grant EAR-9218803 and by the Westinghouse Savannah River Company under subcontract Number AB 46396-0. P.C.R. was also supported by a Laboratory-Graduate Partnership appointment at Argonne National Laboratory. We appreciate the contributions made by Paul V. Roberts in reviewing this work as well as the those made by the anonymous reviewers. Thanks also to Majid Hassanizadeh for his thoughtful comments and editing. We would also like to acknowledge William G. Gray, Carlo Montemagno, and Lin A. Ferrand for their contributions.

### References

- Bear, J., *Dynamics of Fluids in Porous Media*, Dover, Mineola, New York, 1972.
- Blunt, M. J., and P. King, Relative permeabilities from two and three dimensional pore-scale network modeling, *Transp. Porous Media*, 6, 407–433, 1991.
- Blunt, M. J., M. J. King, and H. Scher, Simulation and theory of two-phase flow in porous media, *Phys. Rev. A*, 46(12), 7860–7699, 1992.
- Bryant, S., P. R. King, and D. W. Mellor, Network model of permeability and spatial correlation in a real random sphere packing, *Transp. Porous Media*, 11, 53–70, 1993.
- Burganos, V. N., and A. C. Payatakes, Knudsen diffusion in random and correlated networks of constricted pores, *Chem. Eng. Sci.*, 47(6), 1383–1400, 1992.
- Celia, M. A., P. C. Reeves, and L. A. Ferrand, Recent advances in pore scale models for multiphase flow in porous media, *U.S. Natl. Rep. Int. Union Geod. Geophys. 1991–1994, Rev. Geophys.*, 33, 1049–1057, 1995.
- Chambers, K. T., and C. J. Radke, Capillary phenomena of foam flow through porous media, in *Interfacial Phenomena in Petroleum Recovery, Surfact. Sci. Ser.*, vol. 36, edited by N. R. Morrow, pp. 191–255, Marcel Dekker, New York, 1991.
- Chatzis, I., and F. A. L. Dullien, Application of the theory of percolation for a model of drainage in porous media and relative permeability of injected non-wetting liquid, *Rev. Inst. Fr. Pet.*, 37, 183–205, 1982.
- Chatzis, I., and F. A. L. Dullien, The modeling of mercury porosimetry and the relative permeability of mercury in sandstones using percolation theory, *Int. Chem. Eng.*, 25(1), 47–66, 1985.
- Chatzis, I., N. R. Morrow, and H. T. Lim, Magnitude and detailed structure of residual oil saturation, *SPEJ Soc. Pet. Eng. J.*, 23(2), 311–326, 1983.
- de Arcangelis, L., J. Koplik, S. Redner, and D. Wilkinson, Hydrodynamic dispersion in network models of porous media, *Phys. Rev. Lett.*, 57(8), 996–999, 1986.
- Dias, M. M., and A. C. Payatakes, Network models for two-phase flow in porous media, 2, Motion of oil ganglia, *J. Fluid Mech.*, 164, 337–358, 1986.
- Dullien, F. A. L., *Porous Media: Fluid Transport and Pore Structure*, 2nd ed., Academic, San Diego, Calif., 1992.
- Dullien, F. A. L., F. S. Y. Lai, and I. F. MacDonald, Hydraulic continuity of residual wetting phase in porous media, *J. Colloid Interface Sci.*, 109, 201–218, 1986.
- Fatt, I., The network model of porous media, I, Capillary pressure characteristics, *Pet. Trans. AIME*, 207, 144–159, 1956.
- Ferrand, L. A., and M. A. Celia, Development of a three-dimensional network model for quasi-static immiscible displacement, in *Contaminant Transport in Groundwater*, edited by H. E. Kobus and W. Kinzelback, pp. 397–403, A. A. Balkema, Rotterdam, Netherlands, 1989.
- Ferrand, L. A., and M. A. Celia, The effects of heterogeneity on representative elementary volume size for multiphase porous media (abstract), *Eos Trans. AGU*, 73(14), Spring Meet. Suppl., 123, 1992a.
- Ferrand, L. A., and M. A. Celia, The effect of heterogeneity on the drainage capillary pressure: Saturation relations, *Water Resour. Res.*, 28(3), 859–870, 1992b.
- Fourar, M., S. Bories, R. Lenormand, and P. Persoff, Two-phase flow in smooth and rough fractures: Measurement and correlation by porous-medium and pipe flow models, *Water Resour. Res.*, 29(11), 3699–3708, 1993.
- Geller, J. T., and J. R. Hunt, Mass transfer from nonaqueous phase organic liquids in water-saturated porous media, *Water Resour. Res.*, 29(4), 833–845, 1993.
- Gray, W. G., and S. M. Hassanizadeh, Paradoxes and realities in unsaturated flow theory, *Water Resour. Res.*, 27(8), 1847–1854, 1991a.
- Gray, W. G., and S. M. Hassanizadeh, Unsaturated flow theory including interfacial phenomena, *Water Resour. Res.*, 27(8), 1855–1863, 1991b.
- Gvirtsman, H., and P. V. Roberts, Pore scale spatial analysis of two immiscible fluids in porous media, *Water Resour. Res.*, 27(6), 1165–1176, 1991.
- Haines, W. B., Studies in the physical properties of soils, V, The hysteresis effect in capillary properties and the modes of moisture distribution associated therewith, *J. Agric. Sci.*, 20, 7–116, 1930.
- Hassanizadeh, S. M., and W. G. Gray, Mechanics and thermodynamics of multiphase flow in porous media including interphase boundaries, *Adv. Water Resour.*, 13, 169–186, 1990.
- Hassanizadeh, S. M., and W. G. Gray, Thermodynamic basis of capillary pressure in porous media, *Water Resour. Res.*, 29(10), 3389–3405, 1993a.
- Hassanizadeh, S. M., and W. G. Gray, Toward an improved description of the physics of two-phase flow, *Adv. Water Resour.*, 16, 53–67, 1993b.
- Hillel, D., *Introduction to Soil Physics*, Academic, San Diego, Calif., 1982.
- Hollewand, M. P., and L. F. Gladden, Modelling of diffusion and reaction in porous catalysts using a random three-dimensional network model, *Chem. Eng. Sci.*, 47(70), 1761–1790, 1992.
- Imhoff, P. T., P. R. Jaffe, and G. F. Pinder, An experimental study of complete dissolution of a nonaqueous phase liquid in saturated porous media, *Water Resour. Res.*, 30(2), 307–320, 1994.
- Ioannidis, M. A., and I. Chatzis, Network modelling of pore structure and transport properties of porous media, *Chem. Eng. Sci.*, 48(5), 951–972, 1993.
- Ioannidis, M. A., I. Chatzis, and E. S. Sudicky, A mixed-percolation

- model of capillary hysteresis and entrapment in mercury porosimetry, *J. Colloid Interface Sci.*, *161*, 278–291, 1993.
- Jerauld, G. R., and S. Salter, The effect of pore-structure on hysteresis in relative permeability and capillary pressure: Pore-level modeling, *Transp. Porous Media*, *5*, 103–151, 1990.
- Kantzas, A., and I. Chatzis, Network simulation of relative permeability curves using a bond correlated-site percolation model of pore structure, *Chem. Eng. Comm.*, *69*, 191–214, 1988.
- Koplik, J., S. Redner, and D. Wilkinson, Transport and dispersion in random networks with percolation disorder, *Phys. Rev. A*, *37*(7), 2619–2636, 1988.
- Laidlaw, W. G., W. G. Wilson, and D. A. Coombe, A lattice model of foam flow in porous media: A percolation approach, *Transp. Porous Media*, *11*, 139–159, 1993.
- Lenormand, R., and C. Zarcone, Role of roughness and edges during imbibition in square capillaries, paper presented at the 59th Annual Technical Conference and Exhibition, Soc. of Pet. Eng., Houston, Tex., Sept. 16–19, 1984.
- Li, Y., and N. C. Wardlaw, The influence of wettability and critical pore-throat size ratio on snap-off, *J. Colloid Interface Sci.*, *109*, 461–472, 1986a.
- Li, Y., and N. C. Wardlaw, Mechanisms of nonwetting phase trapping during imbibition at slow rates, *J. Colloid Interface Sci.*, *109*, 473–486, 1986b.
- Li, Y., W. G. Laidlaw, and N. C. Wardlaw, Sensitivity of drainage and imbibition to pore structures as revealed by computer simulation of displacement process, *Adv. Colloid Interface Sci.*, *26*, 1–68, 1986.
- Maier, R., and W. G. Laidlaw, Fluid percolation in bond-site size-correlated three-dimensional networks, *Transp. Porous Media*, *5*, 421–428, 1990.
- Maier, R., and W. G. Laidlaw, Fluid topology for invasion percolation in 3-D lattices, *Transp. Porous Media*, *10*, 221–234, 1993.
- Mayer, A. S., and C. T. Miller, The influence of porous medium characteristics and measurement scale on pore-scale distributions of residual nonaqueous-phase liquids, *J. Contam. Hydrol.*, *11*(3–4), 189–213, 1992.
- Mayer, A. S., and C. T. Miller, An experimental investigation of pore scale distributions of nonaqueous phase liquids at residual saturation, *Transp. Porous Media*, *10*, 57–80, 1993.
- Miller, C. T., M. M. Poirier-McNeill, and A. S. Mayer, Dissolution of trapped nonaqueous phase liquids: Mass transfer characteristics, *Water Resour. Res.*, *26*(11), 2783–2796, 1990.
- Mohanty, K. K., H. T. Davis, and L. E. Scriven, Physics of oil entrapment in water-wet rock, *SPE Reservoir Eng.*, *2*(1), 113–127, 1987.
- Nowicki, S. C., H. T. Davis, and L. E. Scriven, Microscopic determination of transport parameters in drying porous media, *Drying Technol.*, *10*(4), 925–946, 1992.
- Parker, J. C., A. K. Katyal, J. J. Kaluarachchi, R. J. Lenhard, T. J. Johnson, K. Jayaraman, K. Unlu, and J. L. Zhu, Modeling multiphase organic chemical transport in soils and ground water, *Rep. EPA/600/2-91/042*, U.S. Environ. Prot. Agency, Washington, D. C., 1991.
- Payatakes, A. C., K. M. Ng, and R. W. Flumerfelt, Oil ganglion dynamics during immiscible displacement: Model formulation, *AIChE J.*, *26*, 430–443, 1980.
- Powers, S. E., L. M. Abriola, and W. J. Weber Jr., An experimental investigation of nonaqueous phase liquid dissolution in saturated subsurface systems: Steady state mass transfer rates, *Water Resour. Res.*, *28*(10), 2691–2705, 1992.
- Powers, S. E., L. M. Abriola, and W. J. Weber Jr., An experimental investigation of nonaqueous phase liquid dissolution in saturated subsurface systems: Transient mass transfer rates, *Water Resour. Res.*, *30*, 321–332, 1994a.
- Powers, S. E., L. M. Abriola, J. S. Dunkin, and W. J. Weber Jr., Phenomenological models for transient NAPL-water mass-transfer processes, *J. Contam. Hydrol.*, *16*(1), 1–34, 1994b.
- Pyrak-Nolte, L. J., D. Helgeson, G. M. Haley, and J. W. Morris, Immiscible fluid flow in a fracture, in *Rock Mechanics*, edited by Tillerson and Wawersik, pp. 571–578, A. A. Balkema, Rotterdam, Netherlands, 1992.
- Soll, W. E., Development of a pore-scale model for simulating two and three phase capillary pressure–saturation relationships, Ph.D. thesis, Mass. Inst. of Technol., Cambridge, 1991.
- Soll, W. E., and M. A. Celia, A modified percolation approach to simulating three-fluid capillary pressure–saturation relationships, *Adv. Water Resour.*, *16*, 107–126, 1993.
- Sorbie, K. S., and P. J. Clifford, The inclusion of molecular diffusion effects in the network modelling of hydrodynamic dispersion in porous media, *Chem. Eng. Sci.*, *46*(10), 2525–2542, 1991.
- Toledo, P. G., L. E. Scriven, and H. T. Davis, Equilibrium and stability of static interfaces in biconical pore segments, *SPE Form. Evaluation*, *9*(1), 61–65, 1994.
- Tsakiroglou, C. D., and A. C. Payatakes, A new simulator of mercury porosimetry for the characterization of porous materials, *J. Colloid Interface Sci.*, *137*, 315–339, 1990.
- Wardlaw, N. C., and M. McKellar, Oil blob populations and mobilization of trapped oil in unconsolidated packs, *Can. J. Chem. Eng.*, *63*, 525–532, 1985.
- Wardlaw, N. C., and M. McKellar, Mercury porosimetry and the interpretation of pore geometry in sedimentary rocks and artificial models, *Powder Technol.*, *29*, 127–143, 1981.
- Zhou, D., and E. H. Stenby, Displacement of trapped oil from water-wet reservoir rock, *Transp. Porous Media*, *11*, 1–6, 1993.

---

M. A. Celia and P. C. Reeves, Water Resources Program, Department of Civil Engineering and Operations Research, Princeton University, Princeton, NJ 08542. (e-mail: celia@karst.princeton.edu; paul@karst.princeton.edu)

(Received February 6, 1995; revised April 5, 1996; accepted April 8, 1996.)